

# Indentation and acoustic emission in filtration processed platelet reinforced ceramics

P.S. From, R. Pyrz, B. Clausen, E.Ø. Nielsen

*Institute of Mechanical Engineering, Aalborg University, Pontoppidanstræde 101, 9220 Aalborg, Denmark*

Received 3 November 1993; in revised form 7 December 1994

## Abstract

$\text{Al}_2\text{O}_3$ -platelet reinforced zirconia  $\text{ZrO}_2$  composites were fabricated by the filtration method. The elastic constants of composites predicted by the effective medium theory compare very well with experimental values. The fracture toughness of materials was measured by the indentation technique. Incorporation of 5 wt.% platelets in the matrix material increased the fracture toughness by 16% as compared with the pure matrix. During the indentation experiments the acoustic emission activity was monitored, indicating that the indentation crack is formed under increasing loading and it ceases to develop shortly after the indentation force reaches a nominal value. Variations in the acoustic emission energy and the amplitude distribution were related to the crack length and a presence of platelets in the matrix.

*Keywords:* Indentation; Acoustic emission; Platelets; Ceramics

## 1. Introduction

The fracture toughness of the material is of critical importance for the use of ceramic materials in the fabrication of structural elements. Efforts to enhance the fracture toughness include the incorporation of whiskers and fibres in ceramic composites. In comparison to fibres, whiskers have generally a higher toughness and a lower elastic modulus, but they are difficult to disperse evenly in the matrix, forming aggregates of clustered whiskers. Several techniques have been proposed to overcome this difficulty, increasing, however, the overall cost of the final material [1]. Moreover, recent investigations suggest that whiskers can introduce a health hazard similar to asbestos [2]. This has encouraged investigations with alternative reinforcements, such as platelets. Advantages of using platelets instead of whiskers include easier densification, lower cost and environmental safety. Also the toughening ability of platelets should be comparable with that of whiskers provided the size of platelets is well below a critical flaw size [3]. The scarcity of available literature information related to platelet reinforced ceramics points out the need for further investigations of these

materials [4–8]. The aim of this research is to investigate the elastic and the fracture toughness properties of platelet reinforced ceramic composite manufactured by the pressure filtration method. The fracture toughness has been investigated by utilization of the indentation technique. The development of cracks has been accompanied with acoustic emission monitoring in order to explain toughness differences between samples of the matrix material and those having platelet reinforcement.

## 2. Material and manufacturing procedure

The specimens were produced from tetragonal zirconia polycrystal powder  $\text{ZrO}_2$  stabilized with 3 mol.%  $\text{Y}_2\text{O}_3$ . The single-crystal  $\text{Al}_2\text{O}_3$  platelets were used as the reinforcing phase. The platelet size distribution was calculated by dispersing platelets onto a black glass plate and measuring the equivalent diameter of the hexagonal platelets (Fig. 1). The mean diameter of the platelets was 3  $\mu\text{m}$ . The composite suspensions were obtained after 12 h milling of aqueous slurries containing 40 vol.% solids. Two kinds of composites were

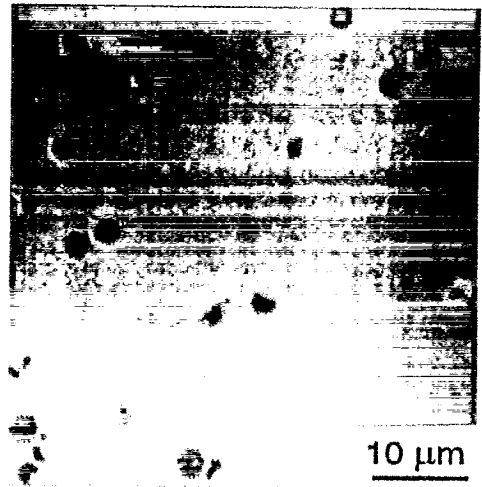
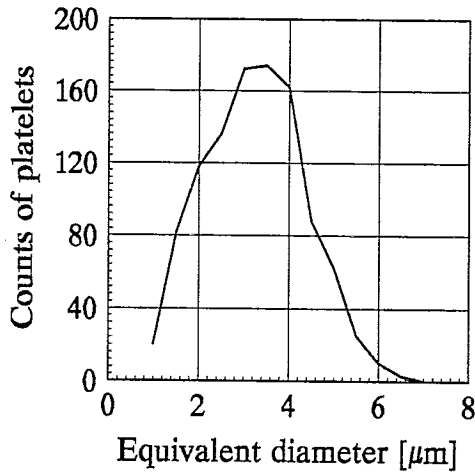


Fig. 1. Metallographic image of platelets and their size distribution.

manufactured with 5 and 10 wt.% platelets, which were dispersed with 0.5 wt.% ammonium carboxylate and 0.25 wt.% polyvinylpyrrolidone. Subsequently, the slurry was placed in the pressure-infiltration device for consolidation during 10 min and under a pressure of 10 MPa (Fig. 2). The “green” specimen was dried first at room temperature for 8 h and finally in an oven for 12 h at 50 °C. After sintering the specimens have a disc form with a diameter of 28 mm and a thickness of 4.8 mm.

3. Results and discussion

The distribution of platelets is fairly uniform both along the thickness of the specimen as well as along the radius of the specimen. However, a slight tendency of a higher concentration has been observed at the bottom surface of the specimen. The orientation distribution of platelets is influenced by eddy texturing, as stated in Ref. [9]. The bulk density of 5 wt.% and 10 wt.% composites amounts to 98.1% and 97.1% of corresponding theoretical densities. These numbers suggest that a residual porosity of samples is negligible.

3.1. Elastic properties

One of the most efficient predictive methods for the determination of elastic constants of composite materials is based on the original derivation of Mori and Tanaka [10], concerned with calculating the average internal stress in a matrix containing precipitates with eigenstrains. This method is frequently used for calculation of effective properties of composites because it yields explicit equations for moduli determination of composites with inclusions of various geometries [11–13].

Assuming the overall homogeneity of platelet distribution, the stiffness tensor of the composite is given by

$$C = C_1 + f_2(C_2 - C_1)T(f_1I + f_2T)^{-1} \tag{1}$$

where the matrix and platelets are labelled by 1 and 2, respectively,  $f$  is the fraction of a corresponding phase,  $I$  is the unit tensor and the concentration tensor  $T$  is written as follows

$$T = [I + EC_1^{-1}(C_2 - C_1)]^{-1} \tag{2}$$

The concentration tensor  $T$  relates the average strain in the interacting inclusions to that of a single inclusion embedded in an infinite matrix subjected to a uniform average matrix strain. The Eshelby tensor  $E$  is calculated for an ellipsoidal inclusion which includes as a special case the disc form of platelets if we assume that two ellipsoidal axes are equal to the mean diameter of platelets, i.e. 3 μm, and the third ellipsoidal axis is equal to the averaged thickness of platelets, 0.6 μm. The explicit expression of the components of the Eshelby tensor  $E$  is given by Mura [13]. The Young modulus of composites has been measured in four-point bending. The mean values from 15 measurements are

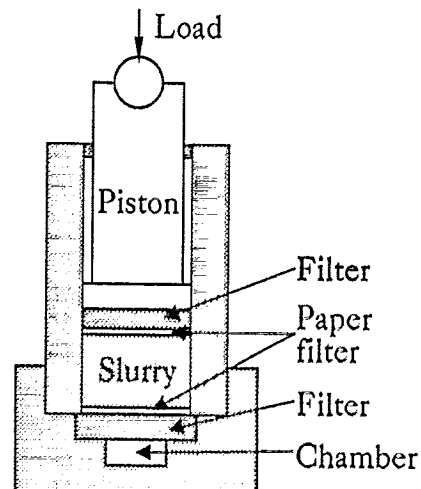


Fig. 2. Filtration set-up.

Table 1  
Elastic constants and flexural strength of constituents and composites

	Matrix	Platelets	Measured 5 wt.%	Calculated 5 wt.%	Measured 10 wt.%	Calculated 10 wt.%
Young modulus (GPa)	206.0 ± 2.0	470	228.0 ± 1.6	220	239.0 ± 0.7	235
Poisson ratio	0.30	0.23	—	0.29	—	0.28
Flexural strength (MPa)	473 ± 53	—	404 ± 58	—	419 ± 45	—

listed in Table 1 together with the results predicted by Eq. (1). Values of the elastic constants of the matrix and the platelets, which are necessary for the calculation of the overall properties of the composites, were supplied by the producer. The platelets are considered as being isotropic. Very good agreement between measured and calculated constants follows from the fact that the elastic properties of two-phase materials are related to lower moments of the local stress distribution, and thus they are practically insensitive to the distribution pattern of inclusions at low inclusion fractions. In such a case one may operate with the average quantities involved in the derivation of Eq. (1).

### 3.2. Fracture toughness

The Vickers indentation technique has been implemented for the measurement of the fracture toughness of composites, after concluding difficulties in obtaining a stable crack growth from pre-notched specimens in four-point bending. The inherent difficulties with Vickers indentation are related to the complex crack pattern nucleated during indentation loading [14–16]. There is a lack of generality in indentation-initiated cracking sequences. Although the crack morphologies observed during the indentation may be categorized as being radial, median, lateral etc., the specific crack sequence in which they form still remains unsolved. This is the reason why only empirical relations exist to evaluate fracture toughness for specific materials and specific types of indentation cracks.

In order to assess the type of crack formed during indentation several experiments have been performed. The indentation has been carried out for six different

indentation forces (Table 2). It has been concluded that the indentation forces above 196 N result in a constant fracture toughness value as calculated from the expression suggested for median cracks [17]

$$K_{IC} = 0.129 \left( \frac{3E}{H} \right)^{2/5} \frac{H\sqrt{a}}{3} \left( \frac{c}{a} \right)^{-3/2} \quad (3)$$

where  $E$  is the Young modulus,  $H$  is the Vickers hardness,  $a$  is the half-diagonal of the Vickers indent and  $c$  is the radius of the crack. The constraint factor is equal to 3. Moreover, the SEM observations have revealed a consistent median crack formation under a force of 491 N. This force value has been used in all subsequent measurements of the fracture toughness. The fracture toughness measurements have been performed for four specimens of each type of composite, with 20 indentation points per sample. The crucial parameter entering Eq. (3) is the crack radius  $c$ , schematically shown in Fig. 3. Its value has been measured with the help of image analysis QUANTIMET 570. The images of cracks have been enhanced by the utilization of the differential interference contrast method (Fig. 4). This method allows for a precise determination of the crack tip which would be blunt otherwise.

Fig. 5 illustrates the dispersion and the orientation of platelets in a typical area of the specimen where the median crack is expected to propagate. The platelets exhibit a tendency towards parallel alignment with the specimen upper surface. This pattern of platelets effec-

Table 2  
Stress intensity factors  $K_{IC}$

Load (N)	$K_{IC}$ matrix (MPa $\sqrt{m}$ )	$K_{IC}$ 5 wt.% (MPa $\sqrt{m}$ )	$K_{IC}$ 10 wt.% (MPa $\sqrt{m}$ )
49	9.25 ± 0.63	11.98 ± 0.85	11.56 ± 0.68
98	6.78 ± 0.34	10.83 ± 0.64	8.99 ± 0.34
196	6.41 ± 0.13	7.72 ± 0.43	7.13 ± 0.55
295	6.45 ± 0.20	7.68 ± 0.70	6.37 ± 0.10
393	6.40 ± 0.28	7.41 ± 0.64	6.97 ± 0.84
491	6.31 ± 0.36	7.31 ± 0.37	7.54 ± 0.53

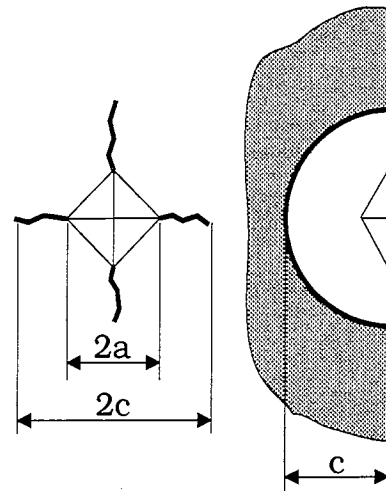


Fig. 3. Top and cross-sectional schematic view of median crack.

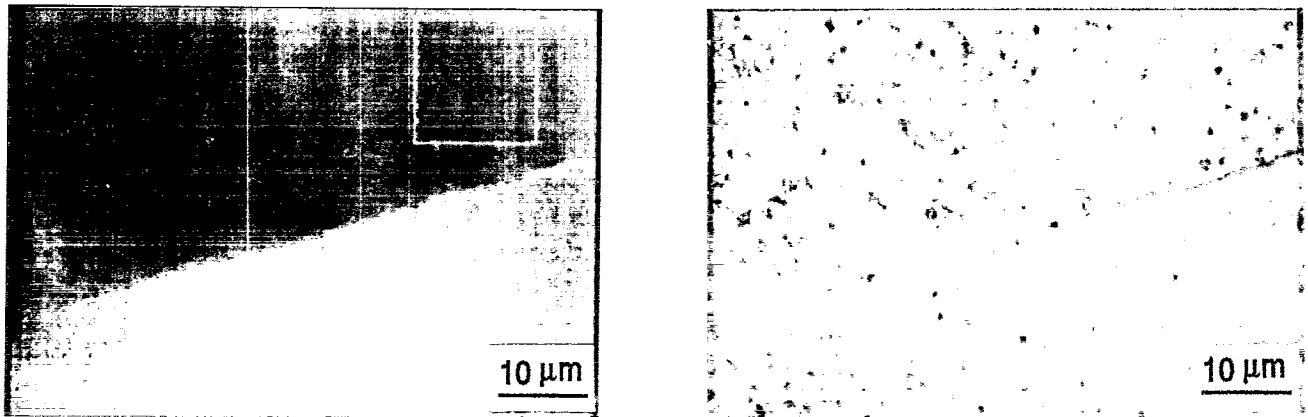


Fig. 4. Surface trace of median crack without (left) and with enhancement (right).

tively influences the crack front only for limited fragments of the angular crack path which are approximately perpendicular to the platelet plane. A more random orientation distribution of platelets would increase the efficiency of the reinforcement [9]. Nevertheless, the stress intensity factor of 5 wt.% composite is 16% larger than the stress intensity factor for the matrix,  $7.31 \pm 0.37 \text{ MPa}\sqrt{\text{m}}$  and  $6.31 \pm 0.36 \text{ MPa}\sqrt{\text{m}}$ , respectively. The increase of the platelets fraction to 10 wt.% only insignificantly improves the fracture toughness,  $7.54 \pm 0.53 \text{ MPa}\sqrt{\text{m}}$ . Simultaneously, the flexural strength of the matrix, which is equal to  $473 \pm 53 \text{ MPa}$ , drops to  $404 \pm 58 \text{ MPa}$  for the 5 wt.% composite (see Table 1).

### 3.3. Acoustic emission

Acoustic emissions (AEs) are generated during transient changes in the local stress field within a material. This useful experimental tool establishes with good accuracy the level of stress required for the onset of

cracking. Some successful attempts to determine the relationship between the characteristics of the acoustic emission radiation and features of a crack have been reported [18–21]. By placing two or more sensors at different positions, an acoustic event would be detected by each sensor at slightly different times, and this difference can be used to calculate the position of the crack front, and the length of the crack and its growth direction can be determined [22]. In the present investigation a wide-band 50–1000 kHz AE transducer has been placed directly on the specimen's surface that is opposite to the indentation surface (Fig. 5). AE signals were transmitted by a 40-dB preamplifier to an acquisition system LOCAN AT6 with a pre-set gain at 20 dB and a threshold value of 45 mV. During the initial, elastic indentation period a small number of AE events is detected in terms of accumulated AE energy, as shown in Fig. 6. These initial events are related to the friction between the indent and the bulk material. An abrupt increase of AE signals is observed during further increases of the indentation force up to its nominal

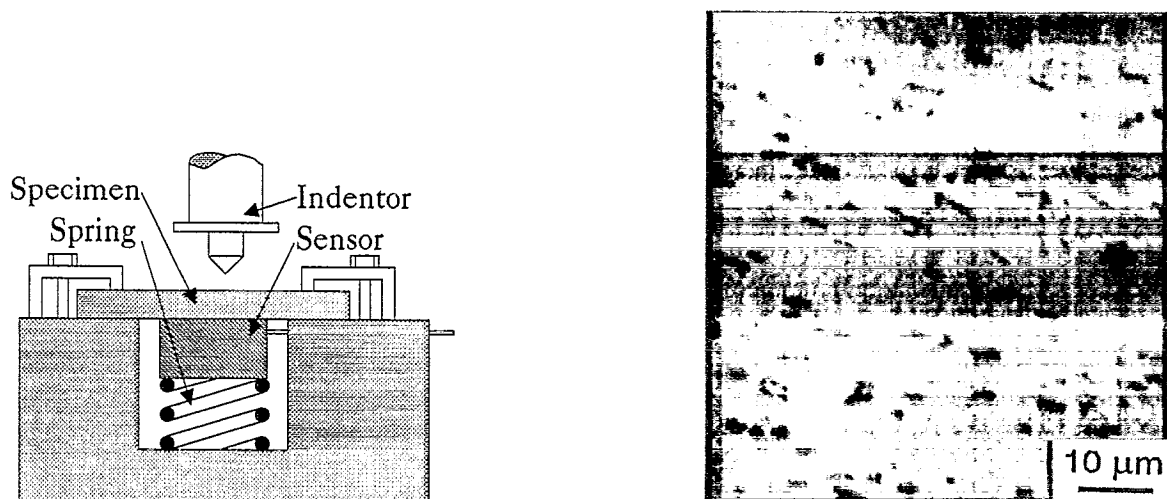


Fig. 5. Distribution of platelets and experimental set-up for acoustic emission measurements.

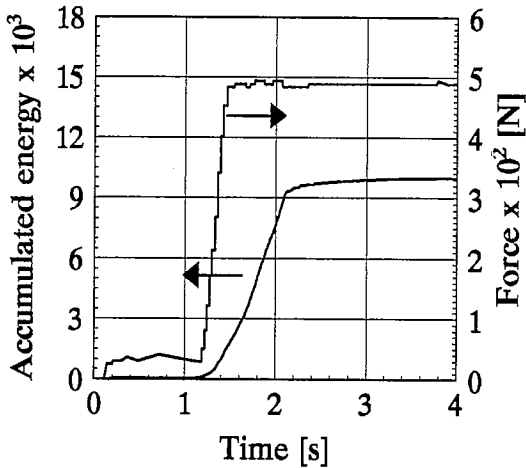


Fig. 6. Indentation force and AE energy at the initial period of loading.

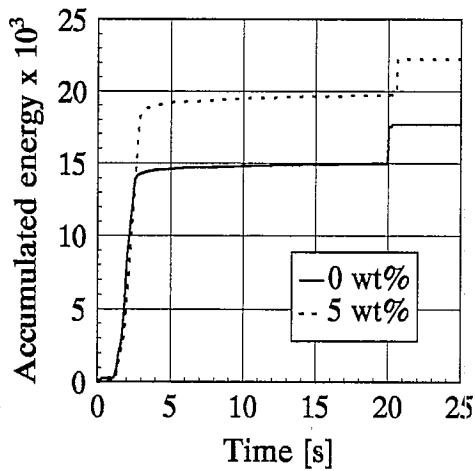


Fig. 7. AE energy during indentation for the matrix and 5 wt.% composite.

value. The acoustic emission events practically cease their propagation under a constant level of the indentation force after a time of 0.6 s. This observation suggests that the hold-time of the indentation does not

significantly influence crack propagation since crack formation takes place almost entirely at the very initial period of the indentation. Fig. 7 presents the amount of accumulated AE energy for the matrix material and the 5 wt.% composite. The increased toughening properties of the composite as compared with the matrix material are exhibited in higher energetics of the AE signals. During unloading the accumulated energy of AE signals grows further due to the friction both on the indent surface and between the closing crack's surfaces. The higher value of the accumulated energy for the composite is caused by the necessity of a crack front to overcome the platelet's barrier. This results in a higher value of dissipated energy as compared with the energy dissipated during the crack propagation in the matrix material specimen. It is interesting to notice that the number of AE events related to the crack length at different indentation forces, as listed in Table 2, is very similar for both materials (Fig. 8). This means that the crack grows in both materials by the same amount of increments which, however, initiate AE bursts of different energies (see Fig. 9). Consequently, the total length of the crack in the composite is shorter than in the matrix specimen under the same indentation force.

The AE amplitude indicates the energetic content of the signal. The cumulative amplitude distribution plot is shown in Fig. 10. The probability of detecting the signal with a preselected amplitude or lower is significantly larger for the matrix material than it is for the composite, and this statement is valid for the whole spectrum of detected amplitudes. This again suggests that the higher amplitude signals are related to the presence of platelets in the matrix material.

#### 4. Conclusions

Platelet reinforced ceramic materials prepared by the filtration technique were examined in this study with

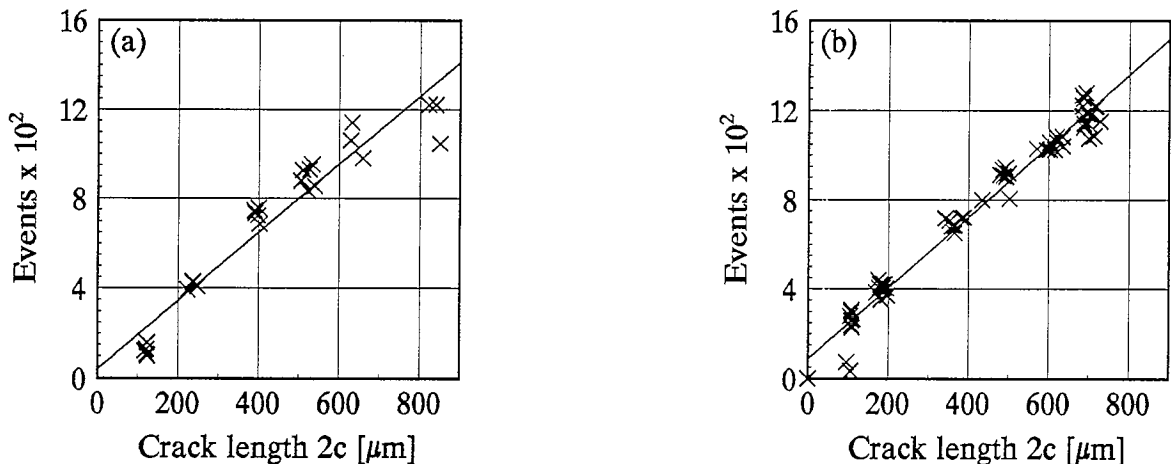


Fig. 8. Plot of events vs. crack length for (a) matrix material and (b) 5 wt.% composite.

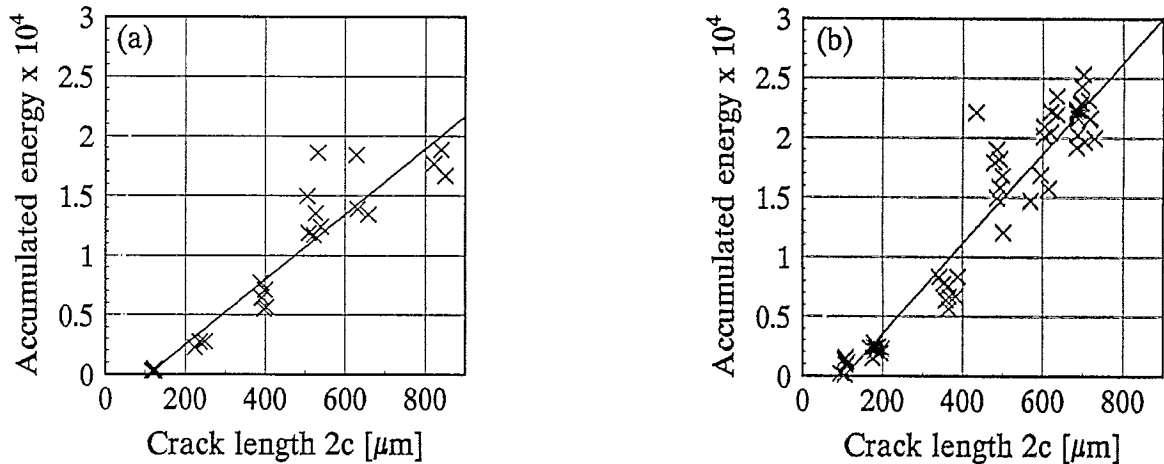


Fig. 9. Plot of AE energy vs. crack length for (a) matrix material and (b) 5 wt.% composite.

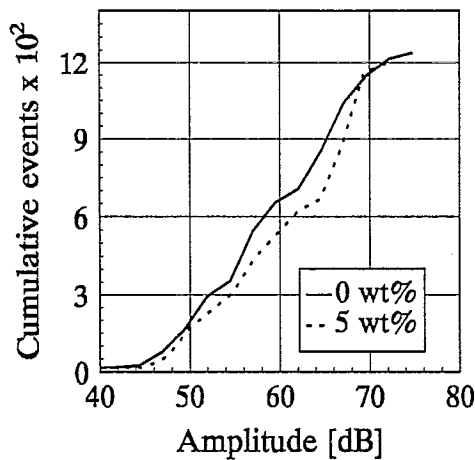


Fig. 10. Cumulative AE amplitude distribution for the matrix and 5 wt.% composite.

respect to their elastic and toughness properties. Very good agreement has been found between predicted values of elastic constants and their experimental counterparts. Reinforcing the  $ZrO_2$  matrix with 5 wt.%  $Al_2O_3$  platelets increased the fracture toughness by 16%, however the incorporation of a larger fraction of platelets does not seem to influence significantly the fracture toughness. The acoustic emission monitoring allows for a clear distinction between the indentation crack lengths in the matrix specimen and the composite. Further effort should be directed towards an extraction of other characteristic parameters from AE signals which would fit more consistently with the crack length. It would ease the determination of the fracture toughness by excluding the time consuming procedure of crack length measurements.

#### Acknowledgement

The authors gratefully acknowledge Dr. Techn. O.T.

Sørensen, Risø National Laboratory, for providing processing facilities.

#### References

- [1] S.A. Gieskes and M. Terpstra (eds.), *Reinforced Ceramic Composites, A Patent Study*, Elsevier Science Publishers, London, 1991.
- [2] J.D. Birchall, D.R. Stanley, M.J. Mockford, G.M. Pigott and P.J. Pinto, *J. Mat. Sci. Lett.*, 7 (1988) 350.
- [3] K.T. Faber and A.G. Evans, *Acta Metall.*, 31 (1983) 565.
- [4] W.B. Johnson, A.S. Nagelberg and E. Braval, *J. Am. Ceram. Soc.*, 74 (1991) 2093.
- [5] E. Breval and W.B. Johnson, *J. Am. Ceram. Soc.*, 75 (1992) 2139.
- [6] D. Baril and M.K. Jain, *Ceram. Eng. Sci. Proc.*, 12 (1991) 1175.
- [7] C. Nischnik, M.M. Seibold, N.A. Travitzky and N. Claussen, *J. Am. Ceram. Soc.*, 74 (1991) 2464.
- [8] N. Claussen, in J.J. Bentzen, J.B. Bilde-Sørensen, N. Christiansen, A. Horsewell and B. Ralph (eds.), *Structural Ceramics Processing, Microstructure and Properties*, Risø National Laboratory, Roskilde, 1990, p. 1.
- [9] D.A. Warner, K.A. Warner, D. Juul Jensen and O.T. Sørensen, in M.I. Mindelson (ed.), *Ceramics Engineering Science*, 1992, p. 172.
- [10] T. Mori and K. Tanaka, *Acta Metall.*, 21 (1973) 571.
- [11] Y. Benveniste, *Mech. Mat.*, 6 (1987) 147.
- [12] T. Chen, G.J. Dvorak and Y. Benveniste, *J. Appl. Mech.*, 59 (1992) 539.
- [13] T. Mura, *Micromechanics of Defects in Solids*, Martinus Nijhoff, The Hague, 1982.
- [14] B. Lawn and R. Wilshaw, *J. Mat. Sci.*, 10 (1975) 1049.
- [15] H. Matzke, *Key Eng. Mat.*, 56–57 (1991) 365.
- [16] R.F. Cook and G.M. Pharr, *J. Am. Ceram. Soc.*, 73 (1990) 787.
- [17] K. Niihara, R. Morena and D.P.H. Hasselman, *J. Mat. Sci. Lett.*, 1 (1982) 13.
- [18] K.Y. Kim and W. Sachse, *J. Appl. Phys.*, 55 (1984) 2847.
- [19] K.Y. Kim and W. Sachse, *J. Appl. Phys.*, 59 (1986) 2704.
- [20] R. Padermanabhan, N. Suriyayothin and W.E. Wood, *Metall. Trans.*, 14A (1983) 2357.
- [21] K.J. Konzstowicz, *J. Am. Ceram. Soc.*, 73 (1990) 502.
- [22] H.H. Moeller, T. Powers, D.R. Petrak and J.E. Coulter, *SAMPE Q.*, 16 (1985) 44.